3E Evaluation and GA-based Multi Objective Optimization of a NH3/H2O Binary Mixture Cycle Fuelled by Solar Energy

M. Sabaghian, F. A. Boyaghchi*

Department of Mechanical Engineering, Alzahra University, Tehran, Iran

A B S T R A C T

Energy, exergy and exergoeconomic (3E) evaluation are performed to assess the performance of a NH_3/H_2O cycle integrated with parabolic trough solar collectors (PTSC). To provide continuous electricity produced by generator when solar beam radiation is insufficient a stabilizer temperature subsystem is utilized. The major thermodynamic parameters and climate conditions variations are selected to investigate, for their effects on the energy efficiency, exergy efficiency and unit cost of electricity of the overall system. The results reveal that the solar collectors exhibit the worst exergy and exergoeconomic performance, so that when system is only fuelled by solar energy, elevation of solar beam irradiation around 40% reduces the efficiencies and electricity production cost within 23% and 0.4%, respectively. It is found that the increment of ammonia basic concentration, turbine inlet pressure, evaporator inlet temperature and evaporator pinch temperature lead to elevation of energy and exergy efficiencies and decrement of electricity production cost. Then, the single and multi-objective optimizations are performed to maximize the energy and exergy efficiencies and minimize the electricity production cost based on genetic algorithm (GA). Results indicate that the electricity production cost obtained through economic optimization is less than around 2% and 2.2% compared to the optimization based on the first and second laws of thermodynamics. Multi objective optimization causes reduction of electricity production cost around 14% and enhancement the energy and exergy efficiencies 8.5% and 6.7%, respectively too.

1. INTRODUCTION

Restrictions of conventional fossil energy resources and environmental impacts have led to suggestion of renewable energy especially solar energy as electricity supplying. Furthermore in today's fast-paced economy and unreliable fuel market, appropriate design and minimizing the costs of energy systems are the main challenges and aims of energy systems engineering. Therefore, there is a need to develop the existing technologies powered by solar energy in aspect of energy saving, economic and environmental indexes.

In recent decades, the technologies assign to the exploitation of low temperature heat sources have been strongly improved and widely increased. The NH_3/H_2O cycle named Kalina is one of the thermodynamic cycle that is becoming a leading technology in solar energy conversion, as a low-temperature cycle. Kalina cycle was proposed firstly by Kalina [1] in 1982. The working fluid of this cycle is ammonia–water mixture which has lower boiling point temperature than water steam; therefore this type of cycles are used as bottoming and low temperature cycle to enhance energy conversion efficiency.

Lately, several researches have been allocated to solar driven Kalina cycles. Lolos and Rogdakis [2] analyzed aKalina cycle operated with flat plate collectors and external heat source. The effects of several parameters on the system performance were eaxamined. Sun et al [3] simulated a Kalina system, based on flat plate collector and an auxiliary super heater, and performed the parameter performance analyses on the system to indicate the relation between mass flow rate of working fluid and system pressure differences. Ganesh and Srinivas [4] investigated a low temperature Kalina cycle driven by solar parabolic trough collectors based on first law of thermodynamics, and studied the effect of thermodynamic parameters on the thermal efficiency to obtain the best condition of system. Wang et al [5] modeled the Kalina cycle operated by compound parabolic collector and thermal storage tank to investigate the effect of turbine inlet pressure and temperature on the net power output in 24 hrs in a

given day. Peng et al [6] proposed a novel triple cycle, including solar gas-turbine cycle driven by parabolic trough collector, the Rankine cycle, and the Kalina cycle as the bottom cycle, to generate power during medium and low insolation periods with no fossil fuel backup. Modi and Haglind [7] studied a Kalina cycle integrated with central receiver solar thermal power plant, that used direct steam generation and compared it with conventional Rankine cycle. Sun et al [8] analyzed energy and exergy rates in the KCS-11 based on solar flat plate collector and an auxiliary super heater, the system also optimized by using the monthly average solar irradiation in Kumejima Island of Japan. Exergoeconomic couples the exergy and economics concepts to appraise and improve the energy systems performances. It provides a manner for appraisal of the unit cost of system products in order to achieve a cost-effective design and operation. Exergoeconomic analysis has been employed in many investigations in order to analyze different types of Kalina cycles.

José and Borgert [9, 10] analyzed and optimized the absorption Rankine and Kalina cycles as bottoming cycle for a cogeneration plant.The result illustrated that using the Rankine cycle increased the net power production about 3.18% and reduced the unitary cost of electricity 3.06%. Valdimarsson and Eliasson[11] investigated factors affecting on the economic index of the Kalina power cycle.

They compared the real life performance of the Kalian and ORC cycle for a typical geothermal condition and established the more appropriate of Kalian cycle. Mirolli [12] studied applications of 6 MW Kalina cycles as a waste heat recovery cycle in cement plant and estimated the simple payback period of cycle less than 4 years. Arslan [13] investigated and optimized the KCS-34 geothermal plant design based on the life-cycle-cost and exergy concepts. Also,the result illustrated that the plant design is economically feasible for the present worth factor higher than 6. Arslan [14] optimized the Kalina cycle system- 34 (KCS-34) economically using an artificial neural network (ANN) for utilization of Simav geothermal field. Also, the cycle was optimized by coupling the determined weights and life-cycle-cost concepts.

Zare et al [15] developed thermodynamic and thermo-economic models of a Kalina cycle to determine the thermodynamic and thermo economic performance. Parametric study and optimization were performed based on thermal efficiency, exergy efficiency and unit cost of the system product. Rodríguez et al [16] used Aspen- HYSYS software simulation to evaluate three different concentrations of the ammonia-water mixture in the geothermal Kalina cycle, based on exergy and economic concepts. Singh and Kaushik[17] analyzed a Brayton–Rankine–Kalina combined power cycle from the exergoeconomic viewpoint. The Specific Exergy Costing (SPECO) methodology was applied to

determine the relevant intervention potential of the system components, then the influence of some decision variables were evaluated on the cycle performance. Zare et al[18] applied the theory of exergetic cost to analyze the combined Gas Turbine-Modular Helium Reactor and waste heat recovery cycle as an ammonia-water power/cooling system. The obtained results indicated that, optimization based on the exergoeconomics, reduced the unit cost of products by 5.4%. Akbari Kordlar et al [19] proposed a combined cogeneration system containing a Kalina cycle. The system was analyzed based on exergoeconomic concept in order to determine the specific exergy cost of the each stream. Kumar Singh [20] applied specific exergy costing (SPECO) approach to evaluate the Kalina cycle combined coal-fired steam power plant.

As appeared in literature review, there is a lack of information in exergoeconomic investigation of Kalina cycle integrated with concentrating parabolic trough solar collectors (PTSC), particularly, the produced power cost which is one of the important aim of thermal system designers. This work is an endeavor to address this lacking of knowledge. For this purpose, the comprehensive energy modeling is developed for PTSC based on Kalogirou [21] and the Specific Exergy Costing (SPECO) approach is applied to the case of a solar driven Kalina cycle in order to find its optimum design conditions. By parametric analyses the effects of decision variables on the thermodynamic and exergoeconomic indexes are determined and then the system is optimized by means of genetic algorithm using the EES software [22].

2. SYSTEM DESCRIPTION

A schematic diagram of the system is shown in Figure 1. The system is divided into three subsystems: Kalina cycle, temperature stabilized and solar collector subsystem. Kalina cycle includes a separator, a turbine, an evaporator, a mixer, a pump, a low temperature (LT) recuperator, a high temperature (HT) recuperator and a condenser. The ammonia-water mixture which has a varying boiling and condensing temperature is used as the working fluid of this cycle. The ammonia-water mixture is heated in the evaporator by absorbing heat from solar collector subsystem (points 1-2). Then, it enters the separator (point 2). The relatively rich solution of ammonia–water is separated from the liquid phase in a separator and leaves the separator as saturated vapor (point 3). Afterward, it passes through the turbine (point 5) and generates power. Saturated liquid of weak solution leaves the separator (point 4) and heats another flow by passing through recuperator (points 4-6). The steam flow (point 5) and liquid flow (point 6) are merged together in mixer to form the ammonia-water basic solution (point 7). After cooling down in LT recuperator (point 8), the mixture is

condensed to liquid phase of ammonia-water (point 9) in the condenser by cooling water (points 19-20). Then it is pumped (point 10) into evaporator after preheating through the LT recuperator (points 10-11) and HT recuperator (points 11-1).

Figure 1. Flow diagram of the Kalina cycle operated by solar energy

TABLE 1. The specifications and design parameters of solar Kalina power plant.

Kalina cycle subsystem	
Pump1 isentropic efficiency	98 %
Pressure losses in the each heat exchanger in kalian cycle	1 bar
Minimum temperature differences in the evaporator	6 K
Minimum temperature differences in the recuperator	5 K
Minimum temperature differences in the condenser	3 K
Turbine isentropic efficiency	87 %
Temperature of the oil at inlet of evaporator	393 K
Temperature of the oil at outlet of evaporator	353 K
Mass rate of ammonia–water mixture to evaporator	16.8 kg/s
Turbine outlet pressure	6.6 bar
Cooling water inlet temperature	278 K
Ammonia content	82 %
Turbine inlet pressure	32 bar
Temperature stabilized subsystem	
Heat transfer efficiency of auxiliary heater	80 %
Volume of thermal storage tank	100 m^3
Area of thermal storage tank	100 m^2
Overall heat transfer coefficient, U	0.001 kW/m^2 K
Solar collector subsystem[23]	
Collector type	Sl3
Concentration Ratio	82
Peak Collector Efficiency	68 %
Annual Thermal Efficiency	53 %
Optical Efficiency	0.8 %
Aperture Area per SCA	545 m^2
Total aperture area	35,970 m^2
Monthly average insolation, H	26.39 MJ/m^2 day

Temperature stabilized subsystem includes a thermal storage tank, an auxiliary heater and a pump. Therminol vp_1 oil is used as the working fluid of this cycle because of its stability in high temperature and good heat transfer properties. Therminol vp_1 heats the ammonia water mixture by passing through the evaporator (point13-14) and then it is pumped to the thermal storage tank (point15). the thermal storage tank

is operated to stabilize the temperature of fluid when solar radiation is not sufficient, in addition an auxiliary heater is installed as the backup energy source to increase the temperature of the working fluid when the fluid's temperature at the outlet of the thermal storage tank (point 12) drops below the allowable temperature to supply the required temperature of fluid in the inlet of evaporator (point 13).

Solar energy collector subsystem includes a pump and the parabolic trough solar collector (PTSC) filed. Therminol vp_1 as the working fluid is pumped to collectors (point 18) and absorbs the solar energy (point 16) to supply the required energy of temperature stabilized subsystem. Table 1. indicates the specifications and design parameters of solar Kalina power plant.

3. THERMODYNAMIC ANALYSIS

Thermodynamic modeling of the solar Kalina system has been conducted based on simulation code in Engineering Equation Solver (EES)[22] to simplify the theoretical analysis, following assumptions are made:

❖ The system operates under a steady state condition.
❖ Heat losses are neglected in pipe lines.
❖ All of the potential and kinetic energies and exergies are ignored.
❖ efficiencies.Pumps and turbines have given isentropic

3.1. Energy Analysis In this section, mass and energy conservation laws are applied to every component of the system and each component is considered as a control volume with corresponding inlet and outlet streams, heat and work transfer. Mass and energy conservation laws are as follows [24]:

$$\sum \dot{m}_{in} = \sum \dot{m}_{out} \tag{1}$$

$$\dot{Q} - \dot{W} = \sum \dot{m}_{in} h_{in} - \sum \dot{m}_{out} h_{out} \tag{2}$$

Here, $\dot{Q}$, $\dot{W}$ and h are heat transfer, work and specific enthalpy of the streams crossing the device boundary.

In the Kalina cycle, ammonia-water mixture is used as the working fluid and ammonia concentration is one of the important parameters in the cycle especially in separator and mixer modeling. Therefore the concentration balance presented for each component is as shown [24]:

$$\sum \dot{m}_{in} x_{in} = \sum \dot{m}_{out} x_{out} \tag{3}$$

Concentrating solar collectors receive only beam solar irradiation. The instantaneous solar beam irradiation, Gb, can be obtained from total solar irradiation, G, as follows [25]:

$$G_B = G - G_d \tag{4}$$

The daily total diffuse radiation, H_d, depending on sunset hour angle ωs, can be obtained from following correlations [26]:

$for : \omega_s \leq 81.4$

$$\frac{H_d}{H} = \begin{cases} 1 - 0.2727K_T + 2.4495K_T^2 - 11.951K_T^3 \\ +9.3879K_T^4 \\ for : K_T < 0.715 \\ 0.143 \, for : K_T \geq 0.715 \end{cases} \quad (5)$$

$for : \omega_s > 81.4$

$$\frac{H_d}{H} = \begin{cases} 1 - 0.2832K_T + 2.5557K_T^2 - 0.8448K_T^3 \\ for : K_T < 0.715 \\ 0.175 \, for : K_T \geq 0.715 \end{cases} \quad (6)$$

Where KT is the daily clearness index [25]:

$$K_T = \frac{H}{H_0} \quad (7)$$

Hourly distribution of solar irradiation from daily total radiation is estimated by following equations. The ratio of hourly total radiation to daily total radiation, rt, is presented as a function of day length, the sunset hour angle ωs and the hour angle ω [25]:

$$r_t = \frac{\pi}{24}(a + b \cdot cos(\omega)) \frac{(cos(\omega) - cos(\omega_s))}{(sin(\omega_s) - \frac{\pi\omega_s}{180} cos(\omega_s))} \quad (8)$$

$$a = 0.409 + 0.5016 \cdot sin(\omega_s - 60) \quad (9)$$

$$b = 0.6609 - 0.4767 \cdot sin(\omega_s - 60) \quad (10)$$

The hourly diffuse Id and the hourly beam radiation I_B is simply obtained from Liu and Jordan correlation [25]:

$$r_d = \frac{\pi}{24} \frac{(cos(\omega) - cos(\omega_s))}{(sin(\omega_s) - \frac{\pi\omega_s}{180} cos(\omega_s))} \quad (11)$$

Energy modeling of the PTSC is based on the equations presented in [21]. According to Figure 2. The incoming solar energy, which is equal to the energy of solar irradiation on the heat transfer fluid (HCE) minus optical losses, is absorbed in HCE at the glass envelope ($q_{3,SolAbs}$) and absorber pipe ($q_{5,SolAbs}$). Most of the absorbed energy by the receiver passes through the absorber pipe material by conduction ($q_{23,cond}$) and finally transferred to (HTF) by convection ($q_{12,conv}$). The remaining energy is dispatched to the glass envelope by radiation ($q_{34,rad}$) and convection ($q_{34,conv}$) and then conducted through the glass envelope wall ($q_{45,cond}$). Along the energy absorption by the glass envelope ($q_{5,SolAbs}$) some of energy is missed by radiation towards the sky ($q_{56,rad}$) and convection to ambient air ($q_{57,conv}$).The energy balance equations of HCE can be expressed as:

$$q_{12, conv} = q_{23,cond} \quad (12)$$

$$q_{3, SolAbs} = q_{34, rad} + q_{34, conv} + q_{23cond} \quad (13)$$

$$q_{34, conv} + q_{34, rad} = q_{45, cond} \quad (14)$$

$$q_{5, SolAbs} + q_{45, cond} = q_{56, rad} + q_{57, conv} \quad (15)$$

$$q_{HeatLoss} = q_{57,conv} + q_{56, rad} \quad (16)$$

Absorption of solar irradiation in the glass envelope is estimated by the following equation:

$$q_{5,SolAbs} = q_{Sol}\eta_{env}\alpha_{env} \quad (17)$$

Here, q_{Sol} and α_{env} are solar irradiance per receiver length units and absorption coefficient of the glass envelopes. η_{env} represents the optical effective efficiency of the glass envelope that relates to optical properties of glass envelope obtained from reference [30]:

$$\eta_{env} = e_{sh}e_{tr}e_{ge}e_{dm}e_{da}e_{un}\rho_{cl}K_\theta \quad (18)$$

Here, K_Θ is the incident angle modifier that is obtained by:

$$K_\theta = cos(\theta) + 0.000884\theta - 0.00005369\theta^2 \quad (19)$$

Also, the absorption of solar irradiation in the absorber is expressed by:

$$q_{3,SolAbs} = q_{Sol}\eta_{Abs}\alpha_{Abs} \quad (20)$$

$$\eta_{Abs} = \eta_{env}\tau_{env} \quad (21)$$
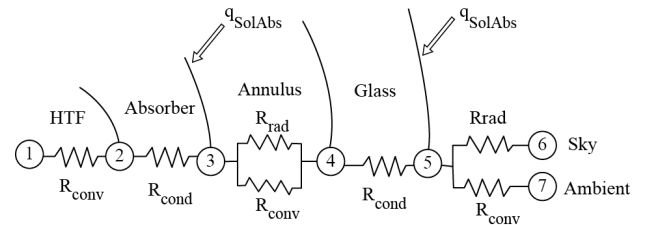
Figure 2. Schematic diagram of heat transfer through HCE components.

As shown in Figure 2. the governing equations in various sections of HCE is explained as follows:
The convection heat transfer from the inner surface of the absorber to the HTF, based on Newton's law of cooling, is given by [130]:

$$q_{12,conv} = h_{f1}\pi D_2(T_2 - T_1) \quad (22)$$

$$h_{f1} = Nu_{D_2}\frac{k_1}{D_2} \quad (23)$$

The Nusselt number is determined by two equations depending on the type of HTF flow. For laminar flow (Reynolds number < 2300), the value of Nusselt number will be 4.36 otherwise in turbulent cases it is calculated by [130]:

$$Nu_{D_2} = Re^{\frac{4}{5}}{}_{D_2} \, Pr_1^{\frac{2}{3}} \qquad (24)$$

Heat transferred by conduction through the absorber pipe wall, is described by the Fourier's conduction law through a hollow cylinder [130]:

$$q_{23,cond} = \frac{2\pi k_{23}(T_2 - T_3)}{ln(\dfrac{D_3}{D_2})} \qquad (25)$$

where k is the conduction coefficient of the absorber.

By considering absorber and glass envelope surfaces as the long concentric isothermal cylinders and gray surfaces, it can be considered that on these surfaces reflections and irradiation is diffuse, so the radiation heat transfer from the absorber to glass envelope is calculated with the following equation [130].

$$q_{34,rad} = \frac{\sigma \pi D_3 (T_3^4 - T_4^4)}{(\dfrac{1}{\varepsilon_3} + (\dfrac{(1 - \varepsilon_4)D_3}{\varepsilon_4 D_4}))} \qquad (26)$$

The convection heat transfer between the outer surface of absorber and inner surface of glass envelope (annulus) is calculated as follows:

$$q_{34,conv} = \pi D_3 h_{f34}(T_3 - T_4) \qquad (27)$$

The convection heat transfer coefficient h_{f34} is assumed to be 0.0001115 [W m^{-2} K^{-1}]

Conduction heat transfer between the glass envelope walls is given by [130]:

$$q_{45,cond} = \frac{2\pi k_{45}(T_4 - T_5)}{ln(\dfrac{D_5}{D_4})} \qquad (28)$$

By considering the glass envelope and the sky as a small convex gray object and large blackbody cavity respectively, radiation heat transfer from the glass envelope to the sky is approximated by [130]:

$$q_{56,rad} = \sigma e \pi D_5 (T_5^4 - T_6^4) \qquad (29)$$

The convection heat transfer from the glass envelope to the atmosphere is presented by Newton's law of cooling [130]:

$$q_{57,conv} = \pi D_5 h_{f57}(T_5 - T_7) \qquad (30)$$

$$h_{f57} = Nu_{D_5} \frac{k_7}{D_5} \qquad (31)$$

The Nusselt number depends on the convection heat transfer mechanism. When it is windy the convection heat transfer is estimated by:

$$Nu_{D_5} = C \, Pr_7^n \, Re_{D_5}^m \, (\frac{Pr_7}{Pr_5})^{1/4} \qquad (32)$$

$$For : 1 < Ra_{D_5} < 10^6, 0.7 < Pr_7 < 500$$

The constants C and m are obtained from reference [30] and the constant n for Pr <= 10 is equal to 0.37 and for

Pr > 10 is equal to 0.36. Following equation is used to estimate the Nusselt number:

$$Nu_{D_5} = \left[0.60 + \frac{0.387 \, Ra_{D_5}^{1/6}}{\{1 + (0.559 / Pr_{57})^{9/16}\}^{8/27}} \right]^2 \qquad (33)$$

$$For : 10^5 < Ra_{D_5} < 10^{12}$$

3.2. Exergy Analysis   Exergy analysis is a tool to develop strategies and guidelines of energy use, therefore resulted in using energy is more effectively. Exergy is represented in terms of four components: Kinetic exergy exKN, potential exergy exPT, physical exergy exPH and chemical exergy exCH [27]. In this study changes in kinetic and potential exergy are neglected.

$$ex_k = ex_{PH,K} + ex_{CH,K} \qquad (34)$$

The physical exergy is the maximum theoretical useful work which is obtained as the system passes from initial state to the dead state[27].

$$ex_{PH,K} = (h_k - h_0) - T_0(s_k - s_0) \qquad (35)$$

Chemical exergy is the exergy component associated with the departure of the chemical composition of a system from that of the environment [28].

$$ex_K^{CH} = \left[\frac{\overline{ex}^0_{CH,NH_3}}{M_{NH_3}} \right] x + \left[\frac{\overline{ex}^0_{CH,H_2O}}{M_{H_2O}} \right] (1 - x) \qquad (36)$$

Here, $\overline{ex}^0_{CH,NH_3}$ and $\overline{ex}^0_{CH,H_2O}$ are standards molar specific chemical exergies of ammonia and water, respectively. The standard chemical exergy of ammonia and water is taken from Kotas [29].

The energy efficiency of the power plant is described as the system's net power output divided by input energy [24], that is supplied by solar collector and auxiliary heater:

$$\dot{W}_{net,out} = \dot{W}_{Tur} - \dot{W}_{P1} - \dot{W}_{P2} - \dot{W}_{P3} \qquad (37)$$

$$\dot{Q}_{in} = (G_B \times A_{ap}) + (\dot{m}_{NG} \times LHV_{NG}) \qquad (38)$$

$$\eta = \frac{\dot{W}_{net,out}}{\dot{Q}_{in}} \qquad (39)$$

The exergy efficiency is defined as the ratio of the actual energy efficiency to the maximum reversible energy efficiency in which both are under the same conditions. The net electrical exergy efficiency is defined as[30]:

$$\varepsilon = \frac{\dot{W}_{net}}{\dot{Ex}_{F,tot}} \qquad (40)$$

Here, $\dot{Ex}_{F,tot}$ is defined as fuel exergy of collectors, $\dot{Ex}_{F,Coll}$ and auxiliary heater $\dot{Ex}_{F,AH}$ which is equal to the system input exergy [31]:

$$\dot{E}x_{F,tot} = \dot{E}x_{F,AH} + \dot{E}x_{F,Coll} \qquad (41)$$

$$\dot{E}x_{F,Coll} = G_B A_{ap}\left(1 + \frac{1}{3}\left(\frac{T_{amb}}{T_{sun}}\right)^4 - \frac{4}{3}\left(\frac{T_{amb}}{T_{sun}}\right)\right) \qquad (42)$$

The exergy from the auxiliary heater is instead calculated as:

$$\dot{E}x_{F,AH} = (\dot{m}_{NG} \times ex_{NG}) \qquad (43)$$

Here, T_{sun} is sun temperature set as 6000 K [25] and ex_{NG} is exergy of natural gas taken about 51.393 kJ kg^{-1} [27].

In order to evaluate the performance of a system from the second law point of view, it is necessary to identify 'fuel–product–loss' (F–P–L) for each component of the system. The product represents the desired result produced by the component or the system. Accordingly, the definition of the product must be consistent with the purchasing and using the system purposes. The fuel represents the resource expended to generate the product, and is not necessarily restricted to being an actual fuel such as natural gas, oil or coal. The losses represent the exergy loss from the system [27]. Exergy destruction for each component of the system can be calculated as follows[27]:

$$\dot{E}x_{D,k} = \dot{E}x_{F,k} - \dot{E}x_{P,k} - \dot{E}x_{L,k} \qquad (44)$$

According to the definition of F-P-L in previous section, the productive structure can be given for each component as follows:

In separator, outlet stream exergy is taken as fuel and inlet streams are considered as product:

Fuel: $\dot{E}x_2$

Product: $\dot{E}x_3 + \dot{E}x_4$

Also the output power of turbine is assumed as its product and the difference between inlet and outlet stream exergy is selected as fuel:

Fuel: $\dot{E}x_3 - \dot{E}x_5$

Product: $\dot{W}_{Tur}$

A bout mixer outlet streams exergy are chosen as product and inlet streams is taken as product:

Fuel: $\dot{E}x_5 + \dot{E}x_6$

Product: $\dot{E}x_7$

For HT and LT recuperators and evaporator we assume that the purpose of the recuperators is to increase the exergy of the cold stream at the exergy of the hot stream expenses .Accordingly, the product and fuel are experessed as follow:

In HT recuperator:

Fuel: $\dot{E}x_4 - \dot{E}x_6$

Product: $\dot{E}x_1 - \dot{E}x_{11}$

In HT recuperator:

Fuel: $\dot{E}x_7 - \dot{E}x_8$

Product: $\dot{E}x_{11} - \dot{E}x_{10}$

And in evaporator:

Fuel: $\dot{E}x_{14} - \dot{E}x_{13}$

Product: $\dot{E}x_2 - \dot{E}x_1$

In the condenser there is exergy stream loss in the environment, and the differences among hot stream exergy are considered as fuel.

Fuel: $\dot{E}x_8 - \dot{E}x_9$

Loss: $\dot{E}x_{20} - \dot{E}x_{19}$

In pumps, the pressure of liquid is increased by means of a mechanical power input. So we consider the product the exergy increase between inlet and outlet stream exergy, and the fuel is the power input. For pump1, pump2 and pump3 the fuels are considered $\dot{W}_{p1}, \dot{W}_{p2}$ and $\dot{W}_{p3}$, respectively and the products are taken as follows:

For pump1: $\dot{E}x_{10} - \dot{E}x_9$

For pump2: $\dot{E}x_{15} - \dot{E}x_{14}$

For pump3: $\dot{E}x_{18} - \dot{E}x_{17}$

Fuel exergy of collectors is equal to collector input exergy and its product is defined as increasing in exergy streams between inlet and outlet of collector[31]:

Fuel: $\dot{E}x_{F,Coll}$

Product: $\dot{E}x_{16} - \dot{E}x_{18}$

In thermal storage tanks, the inlet exergy streams are assumed as fuel and the outlet streams are defined as product. Also the exergy of heat transfer from tank to ambient is considered as loss.

Fuel: $\dot{E}x_{16} + \dot{E}x_{15}$

Product: $\dot{E}x_{12} + \dot{E}x_{17}$

Loss: $U_{TST} A_{TST} (T_{12} - T_{amb}) \times \left(1 - \frac{T_0}{T_{12}}\right)$

For auxiliary heater, the exergy of natural gas are expressed as fuel and increasing in exergy stream between inlet and outlet is taken as product.

Fuel: $\dot{E}x_{16} + \dot{E}x_{15}$

Product: $\dot{E}x_{F,AH}$

4. ECONOMIC AND EXERGOECONOMIC ANALYSES

Thermo-economic combines exergy analysis and economic principles to provide the system designer or operator with information not available through conventional energy analysis and economic evaluations [27]. In this work, specific exergy costing method (SPECO) has been employed for exergy costing analysis of solar driven Kalina cycle. The cost balance at steady state conditions is formulated as following [32]:

$$\sum_{out} \dot{C}_K = \sum_{in} \dot{C}_K + \dot{Z}_K \qquad (45)$$

Here, $\dot{C}$ is the cost rate according to the inlet and outlet streams and $\dot{Z}$ is the capital investment and operating & maintenance cost rate for the kth component. In exergy costing, the inlet and outlet exergy streams of matter $\dot{Ex}_{in,out}$, power $\dot{W}$, and heat transfer $\dot{Ex}_q$ can be written as follows;

$$\dot{C}_{in,out} = c_{in,out} \dot{Ex}_{in,out} \qquad (46)$$

$$\dot{C}_w = c_w \dot{W} \qquad (47)$$

$$\dot{C}_q = c_q \dot{Ex}_q \qquad (48)$$

Here, $C_{in,out,w,q}$ indicates average costs per unit of exergy in \$/kJ for the inlet (in), outlet (out), power (w), and energy (q), respectively.

The annual investment cost rate of each component $\dot{Z}$, is calculated for the desired system. It is the sum of the annual capital investment and the annual operation and maintenance (O&M) cost rates. The total capital investment (TCI) is considered in three parts; direct capital cost (DCC), indirect capital cost (ICC), and other outlays. The total capital investment (TCI) is calculated for each component as 6.32 times the purchase equipment cost (PEC) as given by Bejan et al.[27].

In the present work, the equipment purchasing cost is calculated as function of the components design parameters. The correlations used in this analysis are stated in the form of turbine work output, the volume of thermal storage tank, pumps power, collector field area, heat exchangers surface area, and the heat duty of auxiliary heater. These correlations are formed based on manufacturing data and give the costs in US Dollars. Table 3 expresses these cost functions for each component of the desired system. O&M costs of each component is taken as 25% of the purchase equipment cost [27].

TABLE 3. Cost functions for economic modeling.

System component	Purchased equipment costs function
Heat exchangers [33]	
Evaporator condenser	$3.28 \times 10^4 \times (A/80)^{0.68}$
HT & LT Recuperator	
Pump [33]	$9.84 \times 10^3 \times (\dot{W}/4)^{0.55}$
Collector [34]	$250 \times A$
Thermal Storage Tank [33]	$1.15 \times 10^4 \times (V_{TST}/5)^{0.53}$
Auxiliary Heater [33]	$4.64 \times 10^5 \times (SG/50000)^{0.96}$
Turbine [35]	$4405 \times \dot{W}^{0.7}$

The fuel cost and O&M costs may be vary considerable during system economic life. Therefore levelized annual cost should be performed in cost analysis. The levelized values of fuel cost and O&M costs expenditures can be calculated by multiplying expenditures at the first year by the constant escalation levelization factor CELF[27]:

$$CELF = CRF \cdot \frac{k(1-k^n)}{1-k} \qquad (49)$$

Here, CRF is the capital recovery factor defined as:

$$k = \frac{1+r_n}{1+i_{eff}} \qquad (50)$$

$$CRF = \frac{i_{eff}(1+i_{eff})^n}{(1+i_{eff})^n - 1} \qquad (51)$$

Here, i_{eff} is the effective annual cost of money rate set as 12%, r_n indicates the nominal escalation rate fixed as 5%, and n is the plant lifetime set as 20 years.

Also, the fuel cost rate in auxiliary heater is expressed as levelized cost of natural gas. The cost-balance and auxiliary equations, formulated considering F and P principles [17], for each component of the solar Kalina power cycle. The linear set of cost equations includes 22 unknown variables; $\dot{C}_1$, $\dot{C}_2$,..., $\dot{C}_{19}$, $\dot{C}_{20}$, $\dot{C}_W$ and $\dot{C}_{LOSE,TST}$. In this study we assume a negligible worth for the unit cost of cooling water [36].

5. RESULTS AND DISCUSSION

In this study a comprehensive sensitivity analysis is done to investigate the effect of important factors on thermal and exergy efficiencies and electricity costs. Climate conditions such as solar beam radiation and air temperature as well as thermodynamic parameters namely the turbine inlet and outlet pressures, the inlet and outlet temperatures of evaporator, pinch temperature differences in the evaporator, the basic concentration of ammonia water mixture in the Kalina subsystem are considered for parametric study.

Figure 3. reveals solar irradiation intensity variation effects on the performance of the system considered. It is found that at a given concentration ratio, when the solar beam irradiation increases from 400 to 800 W/m^2, the total incoming exergy to the system and the net power output remain constant. When the solar beam irradiation increases from 400 to 640 W/m^2, the supplied energy and exergy from auxiliary heater decreases and reaches to zero. These variation causes decrement in energy and exergy efficiencies within 0.52% and 0.34%, respectively. When solar irradiation intensity increases from 640 to 800 W/m^2, the total required energy and exergy of the Kalina cycle are supplied only by solar energy. Since the efficiency of the system depends on the collector efficiency, these decrements are significant.

Another implication of Figure 3. is the reduction in the cost of electricity production. In the sensitive analyses of solar irradiation intensities, electricity production cost depends on both the fuel and total exergy destruction cost. By increasing the solar irradiation from

400 to 640 W/m^2 the fuel cost of auxiliary heater decreases from 35.28 to 0 $/h and then it remains constantly close to zero value. The elevation of solar beam irradiance leads to decrease the fuel cost.
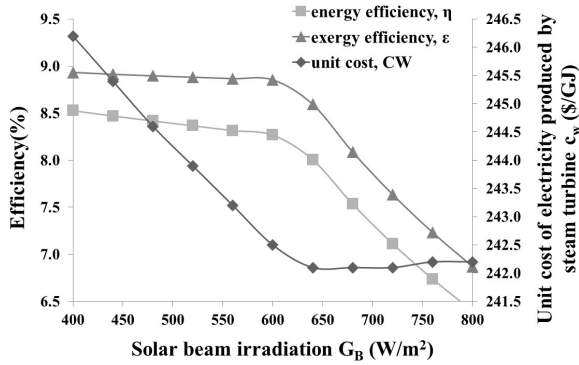
Figure 3. Variation of solar beam irradiation intensity in energy efficiency, exergy efficiency and unit cost of the electricity (x= 0.82 kg/kg, P_3=32 bar, P_5=6.6 bar T_{13}= 393 K, T_{14}=353 K, Δpp_{eva}=6 K)

Also, it increases the cost rate of exergy destruction in the thermal storage tank and collector 130% and 9%, respectively. Therefore, the total exergy destruction cost increases around 144 $/h and the electricity production cost decreases. When the solar irradiation intensity increases from 640 to 800 W/m^2, the fuel cost equals zero, but the total exergy destruction cost increases and leads to increment of electricity production cost.
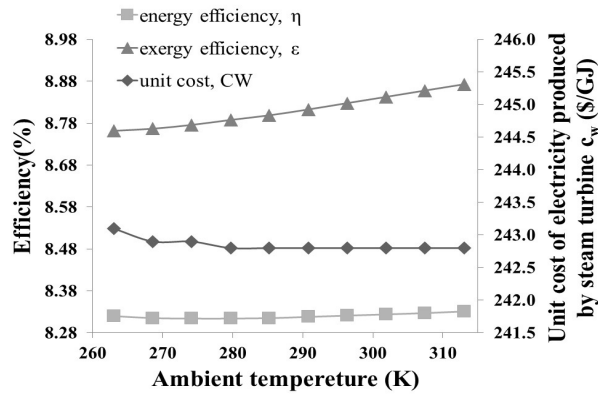
Figure 4. Variation of ambient temperatures on energy efficiency, exergy efficiency and unit cost of the electricity (x= 0.82 kg/kg, P_3=32 bar, P_5=6.6 bar T_{13}= 393 K, T_{14}=353 K, Δpp_{eva}= 6 K)

Figure 4. reveals ambient temperature variation effects on the performance of the system considered. It is found that, when the ambient temperature increases from 263 to 313 K, the thermal efficiency is approximately unchanged while the exergy efficiency increases from 8.76% to 8.87%, because by increasing ambient temperature the total exergy destruction rate decreases around 1.4% that is related to the exergy destruction of collector $Ex_{F,Coll}$, and causes to increase the plant exergy efficiency, but the collector input energy is not

considerable, just 10 kW, and net power output does not change, so the plant energy efficiency reminds approximately constant.

On the other side variation of ambient temperatures on the electricity production cost is low, because the ambient temperature increment, increases the total cost rate of exergy destruction around 1.08 $/h and reduces the capital investment cost within 0.03%. Therefore, interaction of the total exergy destruction cost rate and capital investment decreases the electricity production cost about 0.1% and it remains almost unchanged. Figure 5. shows the effect of the ammonia basic concentration on the thermal efficiency, exergy efficiency and unit cost of electricity production. By increasing the ammonia basic concentration from 0.81 to 0.83 kg/kg when the other parameters are fixed, the exergy and energy efficiencies increase 2.1% and 2.5%, respectively. These increments happen due to increasing the turbine output power (6.4%). Also, elevation of ammonia concentration causes exergy destruction rate increasing in the auxiliary heater and evaporator, so the total exergy destruction rate increases 5.2%. On the other hand, by increasing the ammonia concentration the required energy in the evaporator increases and this causes the increment in Therminol vp_1 mass rate in the temperature stabilized subsystem, so the contribution of auxiliary heater in energy supplying increases. Since the energy and exergy efficiencies of auxiliary heater in energy supplying is more than that for the collector the efficiencies increase, while the total exergy destruction rate and net power output increase too. As the turbine power output increases, the total capital investment and net power output rise about 36 $/h and 136 kW, respectively, also exergy destruction cost decreases 1.3%. These changes decrease the unit cost of electricity production around 4%.
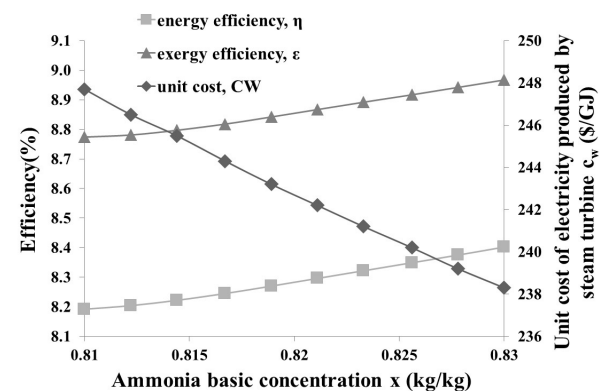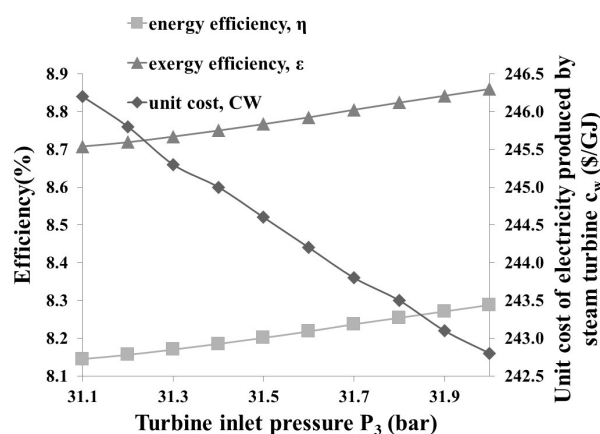

Figure 5. Effect of ammonia basic concentration on energy efficiency, exergy efficiency and unit cost of the electricity (G_B= 582.7 W/m, P_3= 32bar, P_5=6.6 bar, T_{13}= 393 K, T_{14}=353K, Δpp_{eva}= 6 K)

Figure 6. shows the variation of system performances with the turbine inlet pressures. As the turbine inlet pressure increases from 31.1 to 32 bar, the net power

output increases 35 kW. This increment can be attributed to the considerable rise of the turbine output (1.9%). Although increasing the turbine inlet pressure enhances the total exergy destruction rate, Increasing of inlet energy of the system and net power output is more than elevation of total exergy destruction rate. So, increment of net power output causes the growth of thermal and exergy efficiencies 1.4% and 1.5%, respectively. Also, sensitive analysis illustrates that by increasing the turbine inlet pressure around 1 bar, the unit cost of electricity production decreases 3.4 GJ, This variation is mainly due to the fact that the growth of exergy efficiency causes the total cost rate of exergy destruction 2%. On the other hand, an increase in the turbine power output rises the capital investment cost of the turbine from 299.66 to 303.04 $/h, while the decrease in total cost rate of exergy destruction is higher than the increase in the capital investment cost. Therefore, the decrement of exergy destruction cost rate amends the increment of capital investment cost and reduces the system total cost and the electricity production cost.

Figure 6. Effect of the turbine inlet pressure on the energy efficiency, exergy efficiency and unit cost of the electricity (G_B= 582.7 W/m^2, x= 0.82 kg kg^{-1}, P_5=6.6 bar, T_{13}= 393 K, T_{14}=353K, Δpp_{eva}= 6 K)

Effects of the turbine outlet pressure on the system exergoeconomic factors are shown in Figure 7. and 8. As the Figure 7. indicates, by increasing the back pressure of the turbine from 6.5 to 6.8 bar, the total exergy destruction rate increases 96 kW and decrease the turbine net output power about 56 kW. So, design of system in lower turbine back pressure enhances the system's performance, so that by increasing the back pressure of the turbine, the exergy and energy efficiencies decrease about 3%. But, it should be considered that the excessively low back pressure of the turbine causes entering the working fluid in the two-phase region after expansion, and may damage the turbine blade. It can be observed that, with other parameters invariable, when the turbine outlet pressure increases from 6.5 to 6.8 bar, the electricity production

cost increases from 241.7 to 245.4 $/GJ. This increment is expected, owing to increase the total cost rate of exergy destruction about 3 %, because as the turbine outlet pressure increases the total cost rate of exergy destruction increases from 70.2 $/h. On the other hand, increasing in the turbine outlet pressure declines the capital investment cost, but the increment in the cost rate of exergy destruction is higher than decline of the capital investment cost.
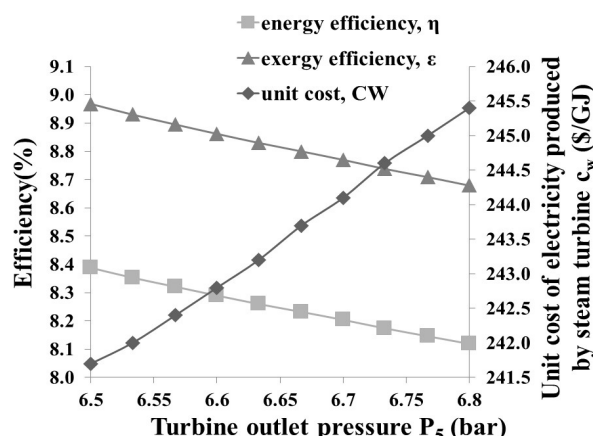

Figure 7. Effect of the turbine outlet pressure on the system exergy destruction rate and the turbine output power (G_B= 582.7 W/m^2, x= 0.82 kg/kg, P_3=32 bar, T_{13}= 393 K, T_{14}=353K, Δpp_{eva}= 6 K)
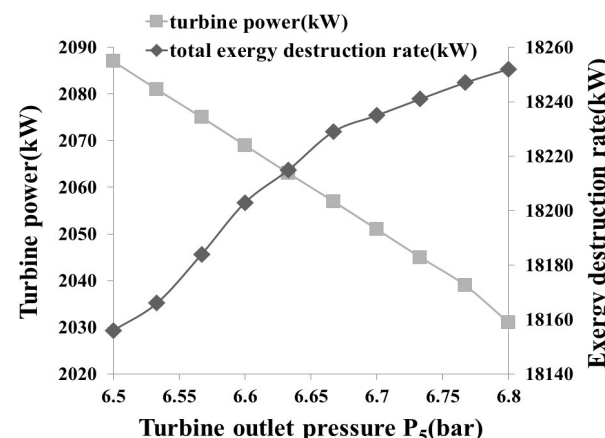
Figure 8. Effects of the turbine outlet pressure on the energy efficiency, exergy efficiency and unit cost of the electricity (G_B= 582.7 W/m^2, x= 0.82 kg/kg, P_3=32 bar, T_{13}= 393 K, T_{14}=353K, Δpp_{eva}= 6 K)

The effect of the evaporator inlet temperature on the system performance is illustrated in Figure 9. As the inlet temperature of the evaporator increases from 390 to 400 K, the turbine outlet power enhances 308 kW and the Therminol vp_1 mass rate decreases from 224 to 197.8 kg/s, so the pump2 power reduces about 23 kW. Also, the enhancement of evaporator inlet temperature increases the fuel consumption in auxiliary heater from 0.008 to 0.06 kg/s and turbine inlet temperature 10 K. These variations cause rise of net power output about

331 kW (19%). This leads to an increment in the thermal and exergy efficiencies by 5.8 and 5%, respectively. Another reason for elevation of efficiencies while the total exergy destruction rate increases is that the contribution of auxiliary heater in energy supplying rises similar to the ammonia concentration variation explained before. Also, the evaporator inlet temperature increment, reduces the total cost rate of exergy destruction around 87.48 $/h, because increasing the evaporator inlet temperature decreases the exergy destruction cost in the evaporator about 4.3%. In addition, the increment of the evaporator inlet temperature reduces mass flow rate of Therminol vp_1 and causes the reduction of exergy destruction cost rate within 2.5% in the pump2. On the other side, rise of evaporator inlet temperature increases the capital investment cost around 1%, but the capital investment increment is less than diminution of exergy destruction cost, therefore, interaction of the total exergy destruction cost rate and capital investment decreases the electricity production cost about 14.7%.
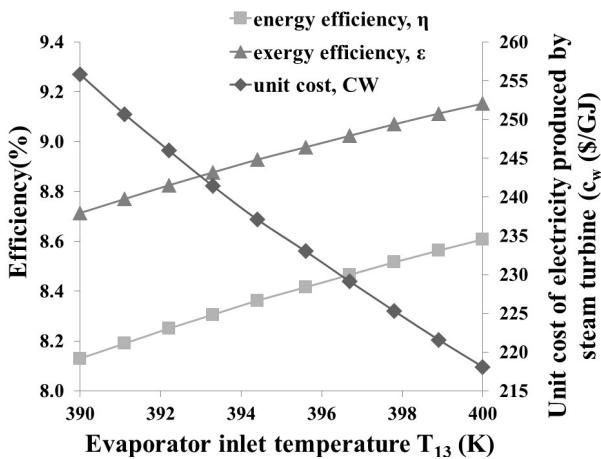
Figure 9. Effects of the evaporator inlet temperature on the energy efficiency, exergy efficiency and unit cost of the electricity (G_B= 582.7 W/m^2, x= 0.82 kg/kg, P_3=32 bar, P_5=6.6 bar, T_{14}=353K, Δpp_{eva}= 6 K)

Figure 10. depicts the relation between the evaporator outlet temperature and the system performance. By increasing the temperature at the outlet of the evaporator from 345 to 380 K, the consumed power of pump2 increases due to elevation of Therminol vp_1 mass flow rate in the temperature stabilized subsystem, so the net power output decreases 429 kW. By increasing the evaporator outlet temperature heat absorption capacity in the evaporator reduces and causes reducing fuel mass flow rate in the auxiliary heater, so the fraction of auxiliary heater in energy supplying dominates and since the efficiency of auxiliary heater in energy supplying is more than that for collector, the thermal and exergy efficiencies decrease 20 %. increasing the temperature at the outlet of the evaporator, would not make considerable change in the total exergy

destruction rate, because it rises in evaporator and pump2 and reduces in thermal storage tank and auxiliary heater, these changes interact together, and hence variation of total exergy destruction rate does not have significant effect on efficiencies. As it can be seen in Figure 10. the evaporator outlet temperature increment increases the unit cost of electricity produced about 20%. This increment can be explained as follows; first, increasing the evaporator outlet temperature elevates the exergy destruction cost in this component around 0.085% while its capital investment cost does not change considerably, second, the mass flow rate of Therminol vp_1 increment causes the growth of exergy destruction cost rate within 0.072% in the pump2. Therefore, these changes cause the increment in total exergy destruction cost.
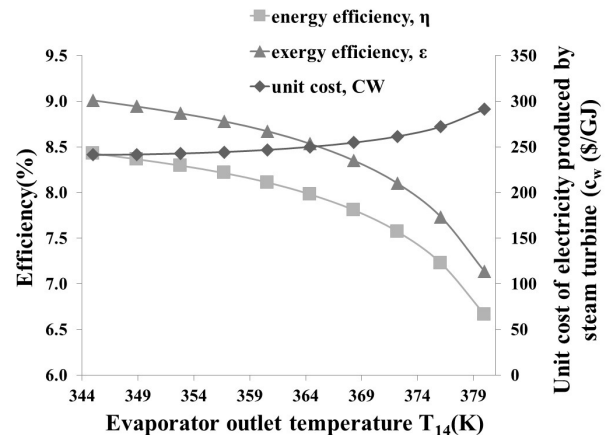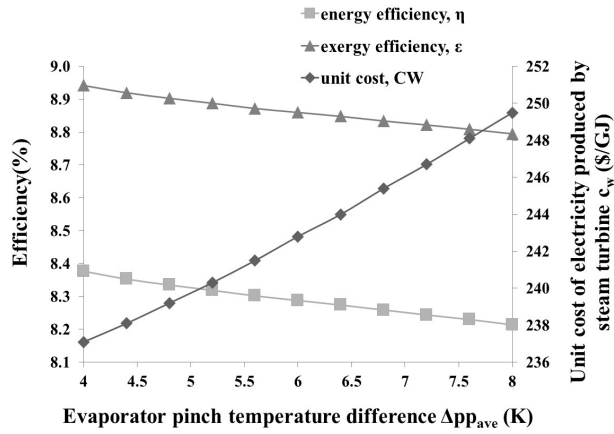

Figure 10. Effects of the evaporator out temperature on the energy efficiency, exergy efficiency and unit cost of the electricity (G_B= 582.7 W/m^2, x= 0.82 kg/kg, P_3=32 bar, P_5=6.6 bar, T_{13}=393K, Δpp_{eva}= 6 K)

The relation between the evaporator pinch temperature difference and system performance is presented in Figure 11. It can be observed that as evaporator pinch temperature difference increases from 4 to 8 K, the energy efficiency decreases from 8.4 to 8.2%. This decrement is due to decrement in the net power output. This variation in net power output can be explained as follows. First, the increasing evaporator pinch temperature difference reduces the turbine inlet temperature and as a result reduction in mass flow rate of ammonia-water mixture vapor about 0.39 kg/s in the evaporator happen, therefore the net power output decreases from 1,901 to 1,785 kW. So, as the pinch temperature difference increases, the thermal and exergy efficiencies decrease 1.9 % and 1.6 %, respectively, due to changes of net power output.

It can also be seen in Figure 11. that as evaporator pinch temperature difference increases from 4 to 8 K, the unit cost of electricity produced by steam turbine remains nearly unchanged (about 12.5 $/GJ), because increment of evaporator pinch temperature difference, increases

the total exergy destruction cost rate and reduces the total capital investment rate, Therefore, the cost of electricity production remains almost stabel due to counter balance of these costs.

Figure 11. Effects of the evaporator pinch temperature difference on the energy efficiency, exergy efficiency and unit cost of the electricity (G_B= 582.7 W/m^2, x= 0.82 kg/kg, P_3=32 bar, P_5=6.6 bar, T_{13}=393K, T_{14}=353K)

5.1. Exergoeconomic optimizati   The performance of the Kalina cycle driven by solar energy is optimized by using the genetic algorithm in EES software. Three output parameters are considered as optimization objectives. these parameters are the unit cost of the system products, thermal efficiency and exergy efficiency while evaporator pinch temperature differences, turbine inlet and outlet pressures, evaporator inlet and outlet temperatures and ammonia basic concentrations are considered as decision variables.

5.2. Optimization method   Various optimization methods are presented in the EES software. Genetic algorithm is the most robust method; hence in this study the genetic algorithm is applied for optimization purposes. Although, the convergent of genetic algorithm is slower than the available methods and it is not influenced by the guess values of the independent variables [37], in some researches, it is obvious that the genetic algorithm is more effective than direct search methods [38]and mathematical approachs [39].

TABLE 4. GA parameters

Parameter	Value
Number of individuals in the population	32
Number of generations	64
Maximum mutation rate	0.2625
Initial mutation rate	0.005
Minimum mutation rate	0.0005
Crossover probability	0.85

For the present study, Table 4. shows the parameters of genetic algorithm in the optimization procedure. The first three parameters can be determined by the EES user. Other parameters are unchangeable within the EES

and have been adjust to the default values of PIKAIA program [37, 40].

5.3. Results Of Single-Objective Optimization
The optimization is carried out for maximizing either the thermal efficiency or exergy efficiency or minimizing the unit electricity production cost considering the restrictions as follows:
Optimize η or ε or c_w(P_3, P_5, T_{14}, T_{13}, x, Δpp_{eva})
Subject to:

$$31.1 \leq P_3\left(bar\right) \leq 32$$
$$6.51 \leq P_5\left(bar\right) \leq 6.8$$
$$345 \leq T_{14}\left(K\right) \leq 380$$
$$390 \leq T_{13}\left(K\right) \leq 400$$
$$0.81 \leq x\left(kg / kg\right) \leq 0.83$$
$$4 \leq \Delta pp_{eva}\left(K\right) \leq 8$$

Table 5. presents the values of objective functions and decision variables for the optimization based on thermal efficiency optimal (TEO), exergy efficiency optimal (EEO) and cost optimal (CO) designs. In addition, values of parameters in the base case and multi objective optimization are also presented in this Table for the compression. One major conclusion which can be observed in results presented in Figure 12. is that exergoeconomic optimization leads to a considerable enhancement in the performance of the system. Figure 12. indicates that, the thermal and exergy efficiencies for the TEO cases are around 9% and 8.6% higher than those for the base case. Also, these variations are 9% and 8.5% for TEE case.
The unit cost of electricity production for the CO case is around 15.6% lower than those for the base case. However the unit cost of electricity production associated with thermodynamically optimal designs is not significantly different from that in the cost optimal design. Also, Figure 12. demonstrates that, in CO case the net power output enhancement is comparable to those of the base case (17.9%). This significant enhancement of the net power output is due to the fact that an elevation of turbine inlet pressure and reduction of turbine outlet pressure result in an increase in the turbine exit power. Also, the higher inlet temperature and the lower exit temperature and pinch difference temperature at evaporator bring about lower exergy destruction, hence it decreases exergy destruction cost and causes increasing the system efficiency and reduces the cost of the electricity.

5.3. Results Of Multi-Objective Optimization
The majority optimization of energy system cases will require the using of multiple objectives optimization.

The cost of a less efficient system is low whereas a system with high efficiency is usually an inexpensive

one, hence, the objectives will be conflicting; The Pareto approach is a conventional method deals with solutions of multi-objective optimization problems. To obtain the most straightforward approach of these problems, the best way is to add each function with determined weight together. For the solar driven Kalina system considered in this work, the combined objective created by summing the three previously mentioned objectives with some proper weights, as follows [41] :

$$Max(MOF = w_1 \times \eta + w_2 \times \varepsilon + w_3 \times (1 - c_w)$$
$$0 \le w_1, w_2, w_3 \le 1$$
$$w_1 + w_2 + w_3 = 1$$

Here, c_w is the unit cost of electricity produced in turbine and w_1, w_2 and w_3 present the weighting coefficients of thermal efficiency, exergy efficiency and , c_w, respectively. All the weighting coefficients are considered equal to 1/3. Results of multi-objective optimization which shown in Figure 12. and Table 5. demonstrate that, if it is important for designer to obtain a high power output, the multi objective optimization is more effective than single objective optimization. Also, multi-objective optimization enhances the energy and exergy efficiencies 8.5% and 6.7%, respectively and reduces the unit cost of electricity production within 14%.

TABLE 5 Optimum values of the objective functions and decision variables for single and multi-objective optimization.

	Base case	CO	TEO	EEO	Multi objective
x (kg/kg)	0.82	0.8297	0.83	0.8299	0.83
P_3 (bar)	32	31.24	31.99	31.99	32
P_5 (bar)	6.6	6.51	6.514	6.514	6.51
T_{13} (k)	393	400	400	399.8	400
T_{14} (k)	353	346.4	346.5	345	346
Δpp_{eva} (K)	6	4.825	4.027	4.034	4
$\dot{W}_{net}$ (kW)	1843	2173	2234	2234	2240
η	0.08343	0.08861	0.09061	0.09053	0.09058
ε	0.08879	0.09283	0.09465	0.09488	0.09477
c_w ($/MJ)	0.243	0.205	0.2092	0.2096	0.2089

6. CONCLUSIONS

This study conducts the parametric study and multi-objective optimization for a Kalina system integrated with PTSC using GA method with three objectives, namely the energy efficiency, exergy efficiency and overall capital costs. Ammonia basic concentration,

turbine inlet pressure, turbine outlet pressure, evaporator inlet temperature, evaporator outlet temperature, evaporator pinch temperature are selected as decision variables due to their significant effects on the objectives.
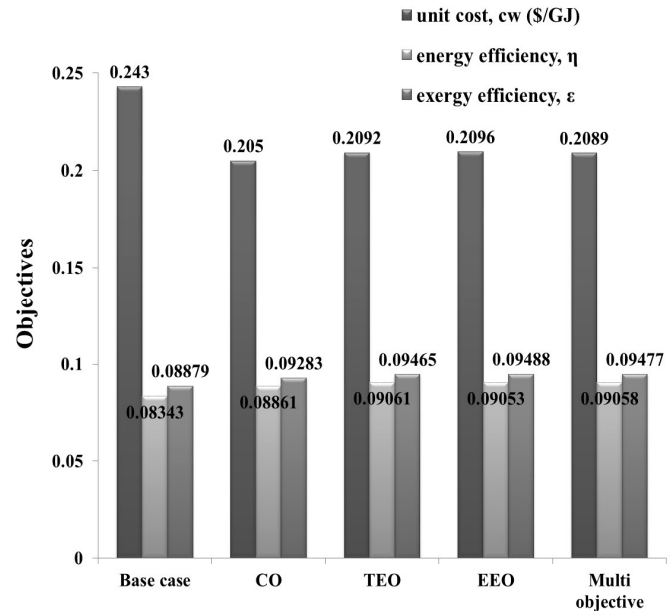
Figure 12. A comparison between single objective and multi-objective optimization.

The major conclusions drawn from the investigation are summarized as follows:
❖ Increasing the solar beam irradiation reduces the system energy and exergy efficiencies by about 2.4% and 2.3%, respectively and reduces the electricity production cost from 246.2 to 242.2 $/GJ.
❖ Increasing the evaporator inlet temperature plays an important role in cost saving, so that its increment decreases electricity production cost within 37.7 $/GJ, but the effect of this parameter on efficiencies is not that significant.
❖ The evaporator outlet temperature is the most influential parameter in system efficiency and electricity cost, so that its decrement improves all these parameters performances.
❖ Ambient temperature and solar irradiation do not have meaningful effect on efficiencies and electricity production costs.
❖ Improvement in single optimization designs in case of energy, exergy and electricity cost optimization are 8.6%, 6.8% and 15.6%, respectively while multi-objective optimization reduces the unit cost of electricity production within 14% and improves the energy and exergy efficiencies 8.5% and 6.7%, respectively.

Nomenclature

A   Area, m^2

$\dot{C}$	Cost rate, $/s
c	Cost per exergy unit, $/kJ
CO	Cost optimal design
EEO	Exergy efficiency optimal design
$\dot{Ex}$	Exergy rate, kW
ex	Specific exergy, kJ/kg
f	Exergoeconomic factor, %
G	Solar irradiation, kW/m
GA	Genetic algorithm
h	Enthalpy, kJ/kg
h_f	Heat transfer coefficient of fluid, W/m^2 K
k	Conductive heat transfer coefficient, W/m K
LHV	Lower heating value, kJ/kg
$\dot{m}$	Mass flow rate, kg/s
Δpp	Pinch temperature difference, K
M	Molecular mass, g/mol
MOF	Multi objective function
n	Total operating period of the system, year
P	Pressure, bar
Pr	Prandtl number
r	Relative cost difference, %
R	Thermal resistance, m K/W
Re	Reynolds number
s	Specific entropy, kJ/kg K
SCA	Solar collector assemblies
SG	Steam generation rate, kg/h
T	Temperature, K
TEO	Thermal efficiency optimal design
V	Volume, m^3
w	Weighting coefficients
x	Ammonia basic concentration

Subscripts

0	Dead states
amb	Ambient
ap	Aperture
b	Beam
D	Destruction
in	Input
net	Net
out	Output

Greek letters

η	Energy (thermal) efficiency
ε	Exergy efficiency, emissivity
θ	Radiation incident angle, $^\circ$
σ	Stefan-Boltzmann constant, $W/m^2 K^4$
ω	Hour angle, $^\circ$

REFERENCES

1. Kalina, A.I., "Generation of energy by means of a working fluid, and regeneration of a working fluid", United States, 1982.

2. Lolos, P.A. and E.D. Rogdakis, "A Kalina power cycle driven by renewable energy sources", *Energy,* Vol. 34, No. 4, (2009), 457-464.

3. Sun, F., Ikegami, Y. and Jia, B., "A study on Kalina solar system with an auxiliary superheater", *Renewable Energy,* Vol. 41, (2012), 210-219.

4. Shankar Ganesh, N. and T. Srinivas., "Design and modeling of low temperature solar thermal power station", *Applied Energy*, Vol. 91, No. 1, (2012), 180-186.

5. Wang, J., Yan, Z., Zhou, E. and Dai, Y., "Parametric analysis and optimization of a Kalina cycle driven by solar energy", *Applied Thermal Engineering,* Vol. 50, No. 1, (2013), 408-415.

6. Peng, S., Hong, H. and Jin, H., "Triple cycle for solar thermal power system adapted to periods with varying insolation", *Energy,* Vol. 60, (2013), 129-138.

7. Modi, A. and Haglind, F., "Performance analysis of a Kalina cycle for a central receiver solar thermal power plant with direct steam generation", *Applied Thermal Engineering,* Vol. 65, (2014), 201-208.

8. Sun, F., Zhou, W., Ikegami, Y., Nakagami, K. and Su, X., "Energy–exergy analysis and optimization of the solar-boosted Kalina cycle system 11 (KCS-11)", *Renewable Energy,* Vol. 66, (2014), 268-279.

9. Borgert Jr, J.A. and Velásquez, J.A., "Analysis of aqua-ammonia power cycles for cogeneration application", *in 17th International Congress of Mechanical Engineering,* (2003).

10. Borgert, J.A. and Velasquez, J.A., "Exergoeconomic optimisation of a Kalina cycle for power generation", *International Journal of Exergy,* Vol. 1, (2004), 18-28.

11. Valdimarsson, P. and Eliasson, L., "Factors influencing the economics of the Kalina power cycle and situations of superior performance", *in International Geothermal Conference, Reykjavik,* (2003), 32-40.

12. Mirolli, M.D., "The Kalina cycle for cement kiln waste heat recovery power plants", *in Cement Industry Technical Conference*, (2005), 330-336.

13. Arslan, O., "Exergoeconomic evaluation of electricity generation by the medium temperature geothermal resources, using a Kalina cycle: Simav case study", *International Journal of Thermal Sciences,* Vol. 49, No. 9, (2010), 1866-1873.

14. Arslan, O., "Power generation from medium temperature geothermal resources: ANN-based optimization of Kalina cycle system-34", *Energy*, Vol. 36, No. 5, (2011), 2528-2534.

15. Zare, V., Mahmoudi, S.M.S., Yari, M. and Amidpour, M., "Thermoeconomic analysis and optimization of an ammonia–water power/cooling cogeneration cycle", *Energy,* Vol. 47, No. 1, (2012), 271-283.

16. Rodríguez, C.E.C., Palacio, J.C.E., Venturini, O.J., Lora, E.E.S., Cobas, V.M., Santos, D.M.D., Dotto, F.R.L. and Gialluca, V., "Exergetic and economic comparison of ORC and Kalina cycle for low temperature enhanced geothermal system in Brazil", *Applied Thermal Engineering,* Vol. 52, No. 1, (2013), 109-119.

17. Singh, O.K. and Kaushik, S.C., "Thermoeconomic evaluation and optimization of a Brayton–Rankine–Kalina combined triple power cycle", *Energy Conversion and Management,* Vol. 71, (2013), 32-42.

18. Zare, V., Mahmoudi, S.M.S. and Yari, M., "An exergoeconomic investigation of waste heat recovery from the Gas Turbine-Modular Helium Reactor (GT-MHR) employing an ammonia–water power/cooling cycle", *Energy,* Vol. 61, No. 1,(2013), 397-409.

19. Kordlar, M.A., Mahmoudi, S.M.S. and Rosen, M.A., "Energy and Exergy Analyses of a New Combined Cycle for Producing Power and Pure Water Using Geothermal Energy", *in 3rd world sustainability Conference*, (2013), 1-23.

20. Singh, O.K. and Kaushik, S.C., "Exergoeconomic analysis of a Kalina cycle coupled coal–fired steam power plant", *International Journal of Exergy*, Vol. 14, (2014), 38-59.

21. Kalogirou, S.A., "A detailed thermal model of a parabolic trough collector receiver", *Energy*, Vol. 48, No. 1, **(**2012), 298-306.

22. Engineering equation solver for microsoft windows Available from: http://www.fchart.com.

23. Baghernejad, A. and Yaghoubi, M., "Exergy analysis of an integrated solar combined cycle system", *Renewable Energy*, Vol. 35, No. 10, (2010), 2157-2164.

24. Sonntag, R.E., Borgnakke, C., "Fundamentals of thermodynamics", (1998): Wiley New York.

25. Kalogirou, S.A., "Solar energy engineering: processes and systems", (2013): Academic Press.

26. Larraín, T., Escobar, R. and Vergara, J., "Performance model to assist solar thermal power plant siting in northern Chile based on backup fuel consumption", *Renewable Energy*, Vol. 35, No. 8, (2010), 1632-1643.

27. Bejan, A., Tsatsaronis, G. and Moran, M., "Thermal design and optimization", (1996), Wiley.

28. Misra, R.D., Sahoo, P.K. and Gupta, A., "Thermoeconomic evaluation and optimization of an aqua-ammonia vapour-absorption refrigeration system", *International Journal of Refrigeration*, Vol. 29, No. 1, (2006), 47-59.

29. Kotas, T.J., "Exergy method of thermal and chemical plant analysis", *Chemical Engineering Research & Design*, Vol. 64, (1986), 212-229.

30. Ahmadi, P., Dincer, I. and Rosen, M.A., "Energy and exergy analyses of hydrogen production via solar-boosted ocean thermal energy conversion and PEM electrolysis", *International Journal of Hydrogen Energy*, Vol. 38, No. 4, (2013), 1795-1805.

31. Petela, R., "Exergy of undiluted thermal radiation", *Solar Energy*, Vol. 74, No. 6, (2003), 469-488.

32. Tempesti, D. and Fiaschi, D., "Thermo-economic assessment of a micro CHP system fuelled by geothermal and solar energy", *Energy*, Vol. 58, (2013), 45-51.

33. Smith, R.M., "Chemical process: design and integration", (2005), John Wiley & Sons.

34. Zhou, C., Doroodchi, E. and Moghtaderi, B., "An in-depth assessment of hybrid solar–geothermal power generation", *Energy Conversion and Management,* Vol. 74, (2013), 88-101.

35. Dorj, P., "Thermoeconomic analysis of a new geothermal utilization CHP plant in Tsetserleg", Mongolia. (2005): United Nations University.

36. Gebreslassie, B.H., Guillén-Gosálbez, G., Jiménez, L. and Boer, D., "Design of environmentally conscious absorption cooling systems via multi-objective optimization and life cycle assessment", *Applied Energy*, Vol. 86, No. 9, (2009), 1712-1722.

37. Klein, S. and Alvardo, F., "EES-Engineering equation solver: user's manual for microsoft windows operating systems", version 8.609, F-Chart Software, Madison, WI, USA, 2009.

38. Maschio, C., Vidal, A.C. and Schiozer, D.J., "A framework to integrate history matching and geostatistical modeling using genetic algorithm and direct search methods", *Journal of Petroleum Science and Engineering*, Vol. 63, (2008), 34-42.

39. Baghernejad, A. and Yaghoubi, M., "Exergoeconomic analysis and optimization of an Integrated Solar Combined Cycle System (ISCCS) using genetic algorithm"*, Energy Conversion and Management*, Vol. 52, No. 5, (2011), 2193-2203.

40. Charbonneau, P., *Release notes for PIKAIA 1.2*. Boulder, Colorado, (2002).

41. Sayyaadi, H., Saffari, A. and Mahmoodian, A., "Various approaches in optimization of multi effects distillation desalination systems using a hybrid meta-heuristic optimization tool", *Desalination*, Vol. 245, (2010), 138-148.